Fibers and Polymers 2015, Vol.16, No.3, 634-639
DOI 10.1007/s12221-015-0634-4

ISSN 1229-9197 (print version)
ISSN 1875-0052 (electronic version)

The Bending Fatigue Comparison between 3D Braided Rectangular Composites and T-beam Composites

Jianhua Yan, Kui Liu[1], Hui Zhou[1], Zhongwei Zhang, Bohong Gu, and Baozhong Sun*

Key Laboratory of Textile Science & Technology Ministry of Education, College of Textiles, Donghua University, Shanghai 201620, China
[1]*Shanghai Aircraft Manufacturing Co., Ltd., Shanghai 200436, China*
(Received May 19, 2014; Revised September 17, 2014; Accepted September 21, 2014)

Abstract: This paper reports the experimental comparison of quasi-static three-point bending and bending fatigue damage behavior between 3D braided rectangular composites (3DBRC) and 3D braided T-beam composites (3DBTC). The stress-deflection curves and failure modes were presented to compare the mechanical properties under quasi-static bending load condition. It was found that the load-carrying capacity of the 3DBTC was much better than that of the 3DBRC, up more than 19 percent. In addition, the S-N curves were employed to illustrate the comparison of fatigue life. The fatigue resistance performance of the 3DBRC was much better than that of 3DBTC at the same stress levels. The increase of of cycle numbers to failure under stress levels of 80 %, 70 %, 60 % and 50 % were 789.6 %, 395.7 %, 48.5 % and 132 %, respectively. The curves of damage indices vs. % of life (n/N×100 %) were given to characterize the three-stage accumulative fatigue failure process for both types of composites. Furthermore, the ultimate failure morphologies were presented to indicate the structural damage modes of the composites under the three-point bending cyclic loading condition.

Keywords: Textile composites, Structural composites, Fatigue, Stress/strain curves, Braiding

Introduction

The aerospace industry has great demand in the applications of three-dimensional (3D) braided composites due to their near-net-shape feature, integrated microstructures and excellent mechanical behavior [1,2]. Comparing with traditional laminate composites, 3D braided composites have a number of advantages including high damage tolerance, through thickness reinforcement and good processability [3].

As one of the key issues on composite materials, the fatigue damage behavior has been widely analyzed by researchers. For 3D textile structural composites, Gowayed and Fan [4] evaluated the fatigue behavior of 3D angle interlock carbon/epoxy woven composites under tension-tension loads. They constructed a mathematical model based on the graphical integrated numerical analysis (GINA) and the results showed a good agreement to experimental data. Carvelli and Lomov [5] studied the tension-tension fatigue behavior of 3D orthogonal E-glass composites and laminated composites reinforced with four plies of plain weave fabrics. The results showed that the 3D woven composite has much longer fatigue life than laminated plain weave composite when loaded in the fill direction. Mouritz [6] found that through-thickness reinforcement is detrimental to the tensile fatigue life by comparing the tensile fatigue properties of specific types of 3D woven, stitched and z-pinned composites. Kelkar *et al.* [7] discussed the biaxial braided carbon/epoxy composites with different braiding angles under tension-tension fatigue loading. Carbon/epoxy unstitched and Z-pinned plain-woven composites were studied under tension-compression fatigue loading. Tate and Kelkar [8] and Tate *et al.* [9] investigated the stiffness degradation model for biaxial braided composites by load-controlled tension-tension fatigue tests. The braided composites revealed substantially different fatigue behavior compared to the conventional angle-ply laminated composites. Liao *et al.* [10,11] explored the tension-tension fatigue and bend-bend fatigue behavior of 3D integral braided carbon/carbon composites (3101 C/C). The load control at a sinusoidal frequency of 10 Hz was used for bend-bend fatigue test to obtain the S-N curves which revealed the relationship between stress and failure cycles. The bending fatigue limit was found to be 203 MPa (92 % of the static flexural strength). Chen [12] and Chen *et al*. [13] presented an approach to predict the delamination of braided carbon fiber lay-up composite T-piece specimen under a mechanical pull-off load case using cohesive models and simulated the multi-directional crack growth in braided laminate T-piece composite specimen. However, as one type of the key cyclic loading conditions of the 3D braided composites, the three-point bending fatigue failure behavior of the 3D braided T-beam has not been well reported so far.

In this paper, a comparative study on the quasi-static three-point bending and bending fatigue damage behavior between 3D braided rectangular composite (3DBRC) and 3D braided T-beam composite (3DBTC) was presented. The global mechanical behaviors of both braided composites were studied, but the effects of material's microstructure were considered because they had similar material microstructure. The stress-deflection curves and failure modes were recorded to compare their mechanical properties under quasi-static loading condition. For the three-point bending fatigue, the S-N curves were provided to show the different fatigue

*Corresponding author: sunbz@dhu.edu.cn

resistance behaviors under various stress levels. Moreover, the three-stage curves of damage index vs. % of life of both types of 3D braided structural composites were presented to show the accumulative fatigue failure process. In addition, the ultimate failure morphologies were also presented to indicate the structural damage modes for both types of composites under three-point bending cyclic loading.

Experimental

Materials

The structure of the four-step 3D braided composite is shown in Figure 1, in which the near-net-shape features and the intergraded microstructure can be observed. The carbon fiber tows (Toray®) were used to fabricate the 3D braided rectangular and T-beam preforms. The specifications of materials are listed in Table 1. The photograph of four-step 3D braided carbon preform is shown in Figure 2.

The vacuum assisted resin transfer molding (VARTM) technique was employed to manufacture the 3D braided composites samples. The matrix was JC-02A epoxy resin provided by JIAFA CHEMISTRY Co., Ltd. in China, the curing agent was JC-02B. The resin solution was prepared by mixing the epoxy resin and curing agent with ratio of 100:80 by weight. The viscosity of the resin solution is 1000-3000 mPa·s at room temperature of 25 °C. The resin solution flowed into the 3D braided perform sample at 40 °C and then cured in oven for 2 hours at a temperature of 90 °C followed by post curing at 110 °C for 1 hour and 130-140 °C for 4 hours. Although the shapes of two types of samples are different, this does not affect the inner structures of the composite. The preform structures and braiding angles are same, so the representative cell for both types of composites are same. That is, the numbers of yarn per unit area in cross-section of both types of samples are same and the fiber volume fractions are same. The fiber volume fraction of both types of composites was approximately 58 % according to the resin burn-off method, described in ASTM D2584. The size of the 3D braided rectangular and T-beam composite samples are shown in Figure 3.

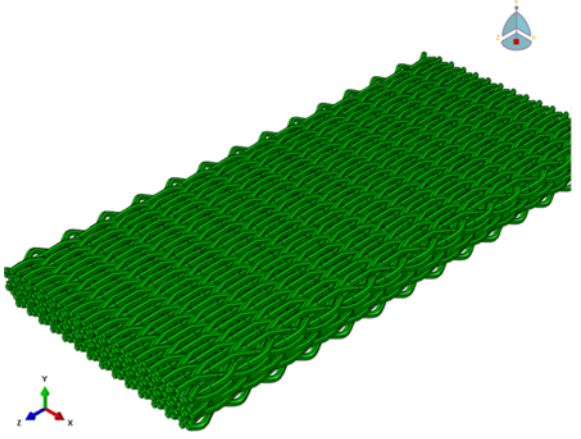

Figure 1. Sketch of the four-step 3D braided composite.

Table 1. Specifications of the 3D braided preforms

	3DBRC	3DBTC
Preform structure	3D four-direction braided	3D four-direction braided
Total number of yarn	145	190
Yarn linear density	12 K	12 K
Braiding angle (°)	30±3	30±3
Stitch length (mm)	2.5	2.5

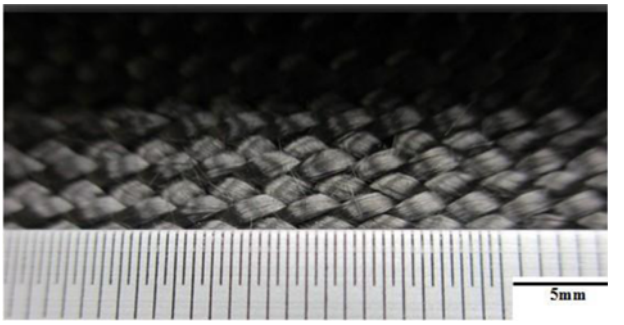

Figure 2. Photograph of the four-step 3D braided carbon preform.

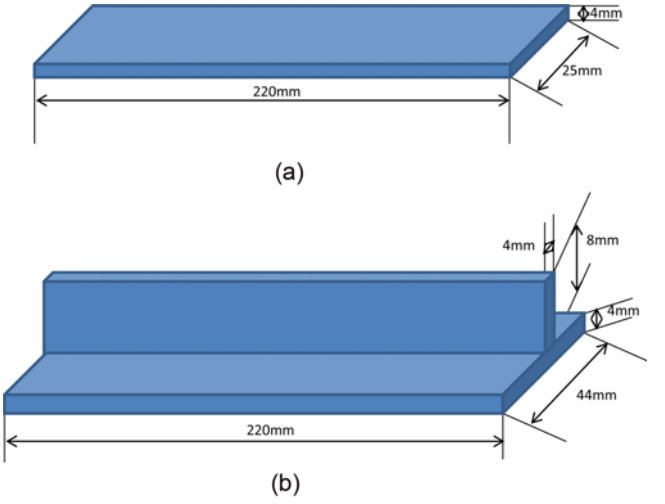

Figure 3. Size of 3D braided rectangular and T-beam composite samples; (a) size of 3D braided rectangular composite sample and (b) size of 3D braided T-beam composite sample.

Quasi-static Bending and Fatigue Tests

As shown in Figure 4, the quasi-static three-point bending test was conducted on the MTS 810.23 material tester at room temperature. One loading roller and two supporting rollers were employed. The size was 20 mm in diameter and

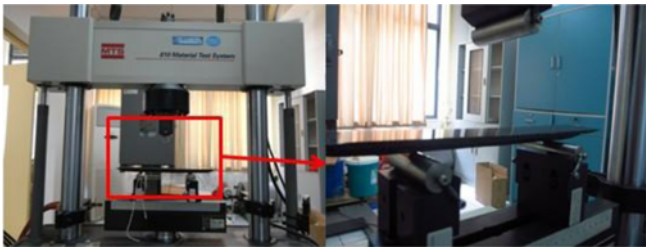

Figure 4. Three-point quasi-static bending and bending fatigue test.

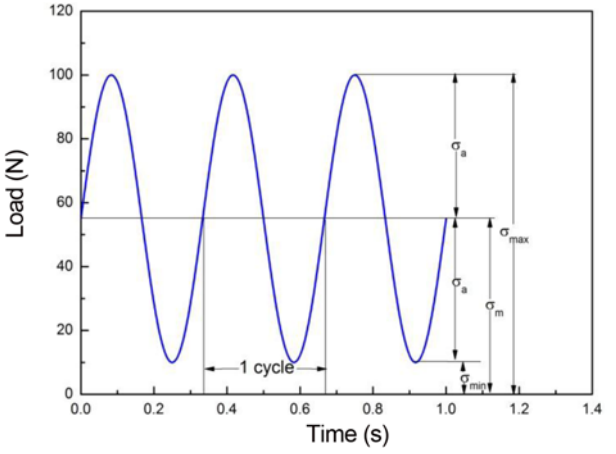

Figure 5. Sinusoidal wave-form cyclic loading used for testing.

70 mm in length. The loading roller was located at the middle of the upper surface of the specimen. The reference standard is ASTM D790.

The three-point bending fatigue tests were also performed on the MTS 810.23 material tester. Figure 5 shows the sinusoidal wave form cyclic loading with a frequency of 3 Hz and stress ratio $\sigma_{f\min}/\sigma_{f\max}$ (ratio of the minimum stress to the maximum stress applied in a single cycle) of 0.1 which was applied on all the tested specimens. The tests on the composites were studied under four different stress levels $\sigma_{f\max}/\sigma_{s\max}$ (ratio of the maximum stress applied in one single cycle to the maximum quasi-static bending stress) of 80 %, 70 %, 60 %, and 50 %.

It is generally known that the loading frequency is one of the most important factors and it affects the fatigue of composites as test temperature. It is further complicated by the change of loading rate, temperature and inhomogeneity of the braided structure. So these factors are not considered, and the fatigues of braided composites are compared just for different cross sectional geometry in this paper.

Results and Discussion

Quasi-static Three-point Bending Load Damage Behavior

3D braided composite has obvious inhomogeneous and anisotropic nature and its yarn traces determines the effective properties. Compared with isotropic materials, the bending properties of composites are complicated. Usually bending tests are the test method for quality control and materials identity rather than what gives you the database of material properties. It is not so easy to explain the bending strength and modulus of 3D braided composites. The mechanical properties of the 3DBRC and 3DBTC specimens under quasi-static three-point bending load in terms of bending modulus (E), ultimate stress (σ_{ult}), and maximum deflection (S) are shown in Table 2. The bending modulus (E_R) and ultimate stress (σ_{ultR}) of 3DBRC were calculated by the equation (1) and (2) [14], respectively. In addition, as the inertia moment of 3DBTC is different from 3DBRC, the bending modulus (E_T) and ultimate stress (σ_{ultT}) of 3DBTC were obtained by equation (3) and (4), respectively.

Table 2. Mechanical parameters of quasi-static bending test

Material type	E (GPa)	σ_{ult} (MPa)	S (mm)
3DBRC	97.6	615	4.3
3DBTC	22.5	764	8.22

$$E_R = \frac{\Delta F \cdot L^3}{\Delta f \cdot 4bh^3} \tag{1}$$

$$\sigma_{ultR} = \frac{3F \cdot L}{2bh^2} \tag{2}$$

where F is the load applied to the specimen, ΔF is the increment of F, Δf is the increment of central deflection, L, b and h are the span between two supporting rollers, width and thickness of the specimen, respectively.

$$E_T = \frac{\Delta F \cdot L^3}{48I \cdot \Delta f} \tag{3}$$

$$\sigma_{ultT} = \frac{F \cdot L \cdot y}{4I} \tag{4}$$

where F is the load applied to the specimen, ΔF is the increment of F, L is the span between two supporting rollers, I is the inertia moment of T-beam composite, Δf is the increment of central deflection, y is the distance between lower surface of web and centroid of T-beam.

It is obviously found that the load-carrying capacity of the 3DBTC is much better than that of the 3DBRC. According to Table 2, the maximum stress of the 3DBTC is up more than 19 percent than that of the 3DBRC. Considering the structure of 3DBTC, the web led to the significantly increase of the flexural rigidity of composite as a common knowledge of mechanics. The web acted as an important part in resisting the bending load during the test. It is not easy for the generation of deformation due to the high inertia moment brought by the web of T-beam composite when the bending stress was applied on specimen. Much more stress was

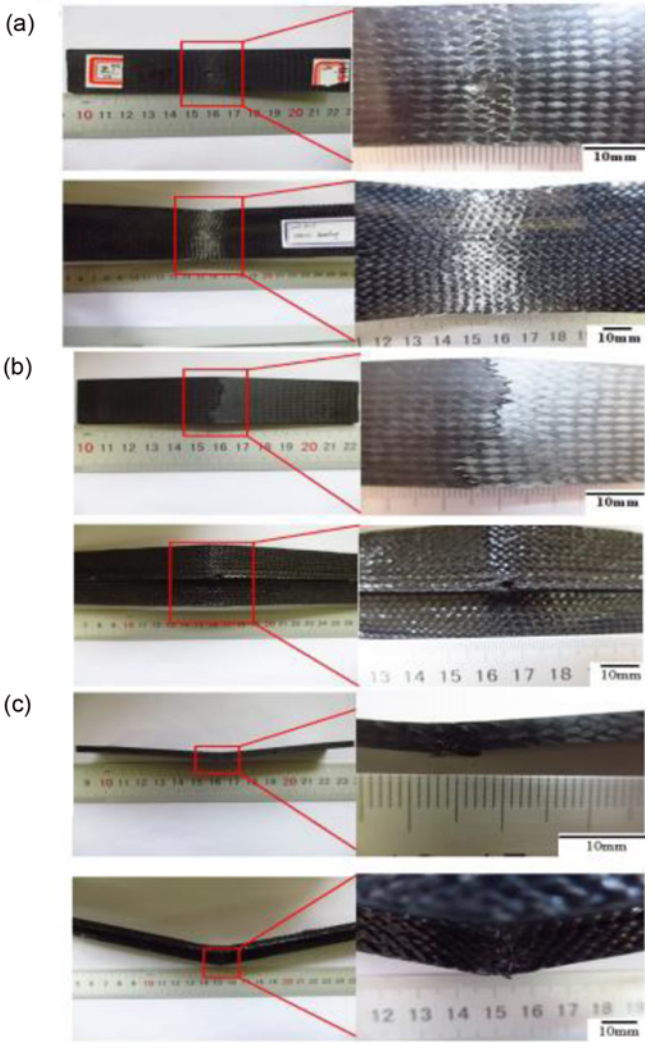

Figure 6. Damage modes after quasi-static tests; (a) upper surface, (b) lower surface, and (c) cross-section.

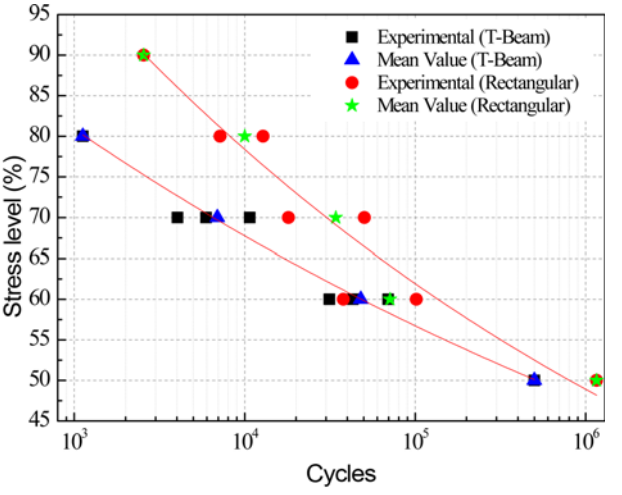

Figure 7. S-N (stress levels vs. number of cycles to failure) curves.

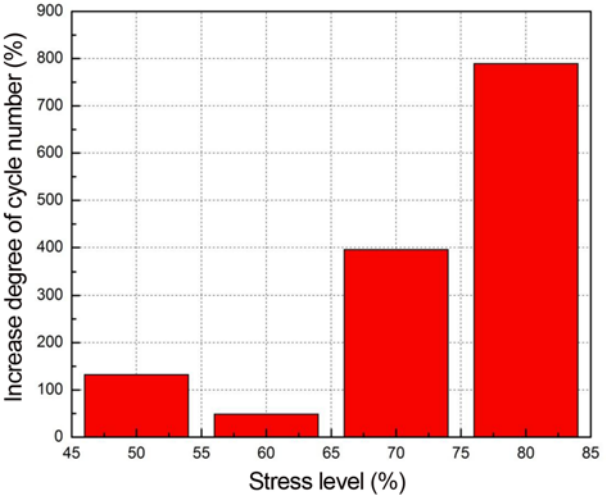

Figure 8. The increase of cycle numbers under corresponding stress level.

required to generate further deformation until the final failure occurred. For the 3DBRC, as the inertia moment is much smaller than that of T-beam composite, the deformation could be generated relatively easier by less stress compared with the 3DBTC. Figure 6 shows damage modes after quasi-static tests.

S-N Curves

Although the through-thickness dimensions between the two composites are very different, and the effect of the stress variation in the thickness direction on the damage initiation and propagation may be different, the global fatigue behaviors can be compared for engineering application. The S-N curves of both types of composites are presented in Figure 7. The 3DBTC and 3DBRC did not fail after over 5×10^5 cycles and 1×10^6 cycles under the stress level of 50 %, respectively. The mean values of numbers of cycles to fatigue failure significantly demonstrate the fatigue life of both types of composites decrease with the increase of the stress level. In addition, it can be found that the fatigue resistance performance of 3DBRC is much better than that of the 3DBTC at the same stress levels which could be obviously found in Figure 8. The increase ($N_{MB}-N_{MT}/N_{MB}$, N_{MB} is the mean cycle numbers of 3DBRC, N_{MT} is the mean cycle numbers of 3DBTC) of cycle numbers to failure under stress levels of 80 %, 70 %, 60 % and 50 % were 789.6 %, 395.7 %, 48.5 % and 132 %, respectively. Therefore, although the web can significantly improve the flexural rigidity, it reduces the tension-loading region area of lower surface during the fatigue test.

D-N Curves

In order to represent the accumulative damage development,

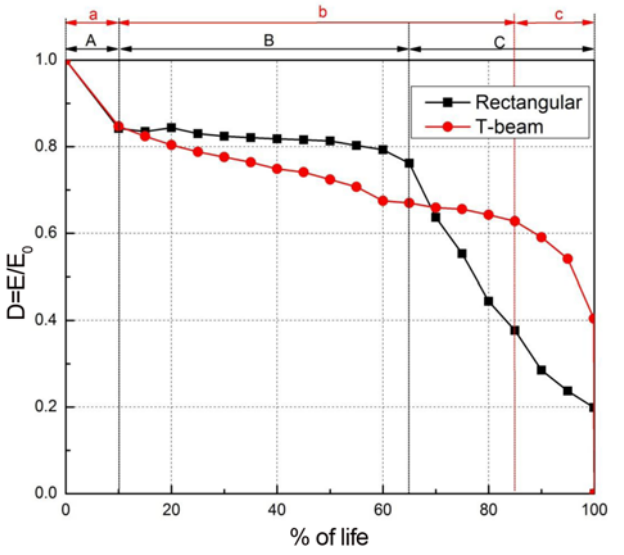

Figure 9. Damage indices vs. % of life of fatigue test under the stress level 60 %.

the fatigue damage indices vs. % of life (n/N×100 %) curves are presented in Figure 9. The fatigue damage index(D) is defined in the term of elastic modulus as expressed in equation (5) [15].

$$D = \frac{E}{E_0} \tag{5}$$

where E is the elastic modulus of the composite material of the specific cycle during fatigue test, E_0 is the elastic modulus of the composite material before fatigue test. D is in the range between 0 and 1 due to E equals to E_0 and 0 as the test begins and ends, respectively.

Three regions, i.e., A, B, and C can be found for both types of composites in Figure 9. Regions A and C correspond to sharp decrease of D within a small amount of testing cycles, region B corresponds to a tiny continuous decrease of D during a large amount of testing cycles. This is the presentation of accumulative fatigue damage development of the braided composite specimens subjected to cyclic loading as described below.

In region A, the initiation and propagation of matrix cracks is the primary damage mode. Once the cyclic load was applied on the surface of composite specimen, the matrix cracking began to occur at the central part of the specimen when the initiation crack threshold was attained after a certain number of testing cycles. The cracks propagated into the inner of sample as the loading process went on which resulted in the sharp degradation of stiffness of the composite specimen. This procedure occupied a relatively smaller amount of testing cycles and correspondingly the first sharp decrease of D.

In region B, the cracks continued to propagate from outer surface to the inner surface of the specimen until the process of fatigue damage turned into region B, and the propagation of cracks entered into yarns near the outer surface as a result of stress concentration. During this process, the interface debonding of matrix-yarns took place due to the persistent propagation of cracks. This procedure consumed relatively much more cycles, which lead to further degradation of stiffness of the specimens and a slow persistent decrease of D.

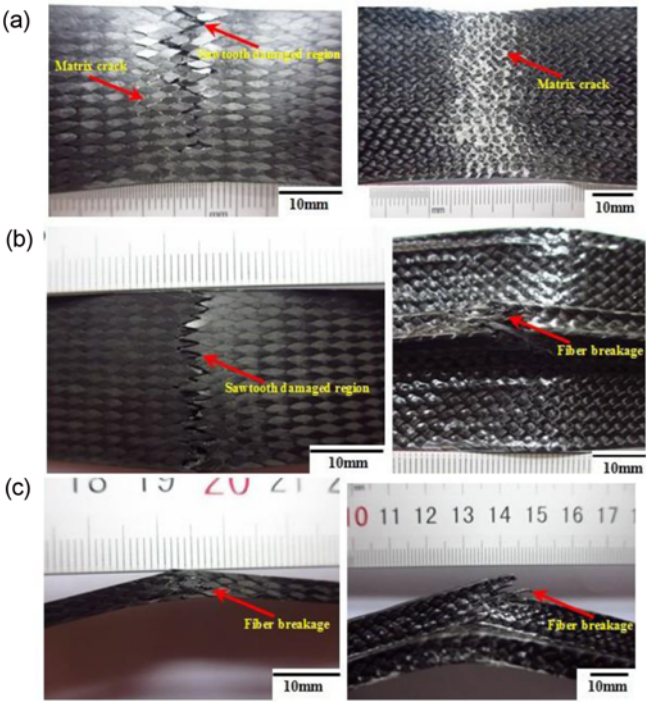

Figure 10. Fatigue damage morphologies. Left: 3DBRC, right: 3DBTC; (a) the upper surface, (b) the lower surface, and (c) the side view.

In region C, it is the progressive breakages of yarns at the outer surface. The piecemeal breakages of yarns were emerged with the proceeding of testing cycles until the ultimate failure occurred. This accumulative damage process also consumed a small amount of testing cycles and corresponding to a sharp decrease of D.

Fatigue Failure Modes

The fatigue damage morphologies of the 3DBRC and the 3DBTC specimens on the basis of the upper, side and lower surfaces are shown in Figure 10.

Two saw-toothed damaged regions could be found from Figure 10(a) and (b), which exist on the central part of the upper surface and lower surface of the 3DBRC specimen. Both regions are located at the positions of stress concentration where subjected to compression load and tension load, respectively.

For the 3DBTC, damaged region could also be found at

the cross-section and lower surfaces, which locates at the central place of the specimen as well. These appearances showed that the central part where is the direct load-carrying areas is the critical regions of stress concentration in the 3DBTC structure. And it is easy for generating cracks in such type of structures. From the damaged side view of both types of composites, the damage shows the similar morphologies on fiber tows breakage. However, for 3DBRC, almost all fibers of the loading-carrying central area emerged fiber breakage which led to the ultimate failure. As for 3DBTC, the fiber breakage just be found at the web.

Conclusion

The quasi-static three-point bending and bending fatigue failure behavior of 3DBRC and 3DBTC were compared and analyzed. It was found that both the distribution and area of damage regions presented significant differences. The 3DBTC could sustain more quasi-static bending loads but hold relatively shorter period of fatigue life under the selected stress levels compared with the 3DBRC. The structural difference between these two types of composites, i.e., the existence of the web of 3DBTC, acted as key role under both quasi-static bending and cyclic bending load conditions. Furthermore, the three-stage accumulative damage development was the dominating failure mechanism for both types of composites under three-point bending fatigue load.

Acknowledgements

The authors acknowledge the financial supports from the National Science Foundation of China (Grant Number 11272087). The financial supports from the Foundation for the Fok Ying-Tong Education Foundation (Grant No. 141070), the Keygrant Project of Chinese Ministry of Education (No 113027A), Shanghai science and technology innovation action plan (grant no. 12521102400 and 12dz1100407). Funds for National Engineering and Research Center for Commercial Aircraft Manufacturing and the Fundamental Research Funds for the Central Universities of China are also gratefully acknowledged.

References

1. C. P. Pastore, *Mech. Compos. Mater.*, **36**, 97 (2000).
2. J. Lyons and C. M. Pattore, *Fiber. Polym.*, **5**, 182 (2004).
3. L. Chen, X. M. Tao, and C. L. Choy, *Compos. Sci. Technol.*, **59**, 391 (1999).
4. Y. Gowayed and H. Fan, *Polym. Compos.*, **22**, 762 (2001).
5. V. Carvelli, G. Gramellini, S. V. Lomov, A. E. Bogdanovich, D. D. Mungalov, and I. Verpoest, *Compos. Sci. Technol.*, **70**, 2068 (2010).
6. A. P. Mouritz, *Compos. Sci. Technol.*, **68**, 2503 (2008).
7. A. D. Kelkar, J. S. Tate, and R. Bolick, *Mater. Sci. Eng. B-Adv. Funct. Solid-State Mater.*, **132**, 79 (2006).
8. J. S. Tate and A. D. Kelkar, *Compos. Pt. B-Eng.*, **39**, 548 (2008).
9. J. S. Tate, A. D. Kelkar, and J. D. Whitcomb, *Int. J. Fatigue*, **28**, 1239 (2006).
10. X. L. Liao, H. J. Li, W. F. Xu, and K. Z. Li, *Sci. China Ser. E.*, **50**, 97 (2007).
11. X. L. Liao, H. J. Li, W. F. Xu, and K. Z. Li, *Compos. Sci. Technol.*, **68**, 333 (2008).
12. J. Chen, *Fatigue Fract. Eng. Mater. Struct.*, **34**, 123 (2011).
13. J. Chen, E. Ravey, S. R. Hallett, M. R. Wisnom, and M. Grassi, *Compos. Sci. Technol.*, **69**, 2363 (2009).
14. H. Hu, M. Zhang, R. Fangueiro, and M. D. Araujo, *J. Compos. Mater.*, **44**, 1753 (2010).
15. Q. Zhao, L. Jin, L. Jiang, Y. Zhang, B. Sun, and B. Gu, *J. Reinf. Plast. Compos.*, **30**, 1571 (2011).